

# Tectonics

## RESEARCH ARTICLE

10.1029/2020TC006425

### Key Points:

- Seismic reflection profiles in the northern Adriatic Sea allow to reconstruct the Apennines fold-thrust belt geometry and its foreland
- Offshore CGPS data allow computation of the active shortening in the accretionary prism
- Analytical modeling provides a first-order estimation of the current slip rate of the unlocked and locked surfaces of the basal decollement

### Supporting Information:

- Supporting Information S1

### Correspondence to:

G. Pezzo,  
giuseppe.pezzo@ingv.it

### Citation:














Pezzo, G., Petracchini, L., Devoti, R., Maffucci, R., Anderlini, L., Antoncicchi, I., et al. (2020). Active fold-thrust belt to foreland transition in northern Adria, Italy, tracked by seismic reflection profiles and GPS offshore data. *Tectonics*, 39, e2020TC006425. <https://doi.org/10.1029/2020TC006425>

Received 9 JUL 2020

Accepted 7 OCT 2020

Accepted article online 9 NOV 2020

## Active Fold-Thrust Belt to Foreland Transition in Northern Adria, Italy, Tracked by Seismic Reflection Profiles and GPS Offshore Data

G. Pezzo<sup>1</sup> , L. Petracchini<sup>2</sup>, R. Devoti<sup>1</sup> , R. Maffucci<sup>3</sup> , L. Anderlini<sup>4</sup> , I. Antoncicchi<sup>5,6</sup>, A. Billi<sup>2</sup> , E. Carminati<sup>3</sup> , F. Ciccone<sup>5,7</sup>, M. Cuffaro<sup>2</sup> , M. Livani<sup>3</sup>, M. Palano<sup>8</sup> , P. Petricca<sup>3</sup> , G. Pietrantonio<sup>1</sup> , F. Riguzzi<sup>1</sup> , G. Rossi<sup>5,6</sup>, F. Sparacino<sup>8</sup> , and C. Doglioni<sup>1,3</sup> 

<sup>1</sup>Istituto Nazionale di Geofisica e Vulcanologia, Osservatorio Nazionale Terremoti, Rome, Italy, <sup>2</sup>Consiglio Nazionale delle Ricerche, IGAG, Rome, Italy, <sup>3</sup>Dip. Scienze della Terra, Sapienza Università di Roma, Rome, Italy, <sup>4</sup>Istituto Nazionale di Geofisica e Vulcanologia, Sezione di Bologna, Bologna, Italy, <sup>5</sup>Ministero dello Sviluppo Economico MiSE, DGS-UNMIG, Rome, Italy, <sup>6</sup>Research on Energy System RSE S.p.A, Milan, Italy, <sup>7</sup>Consiglio Nazionale delle Ricerche, Istituto di Scienze Marine ISMAR, Bologna, Italy, <sup>8</sup>Istituto Nazionale di Geofisica e Vulcanologia, Sezione di Catania, Catania, Italy

**Abstract** The Adria microplate is the foreland of the oppositely verging Apennines and Alps or Dinarides fold-thrust belts associated to the related subduction zones. Along its western margin, the Adria plate hosts the active Northern Apennines accretionary prism, which is buried under the Adriatic Sea and the Po Plain. The interpretation of seismic reflection profiles and borehole data allowed us to define the geometry of the transition from the Apennines fold-thrust belt to its undeformed foreland. Moreover, continuous GPS (CGPS) data from offshore hydrocarbon platforms anchored to the seabed of the northern Adriatic plate allow to measure present-day kinematics. Although the CGPS signals are affected by non-tectonic components associated with hydrocarbon extraction, the integration of geodetic analysis, subsurface geological reconstructions, and analytical modeling allowed us to constrain the ongoing tectonic activity. Shortening is currently accommodated by aseismic slip along the basal detachment, likely accumulating elastic energy along the frontal ramp that may eventually seismically slip. Our multidisciplinary study suggests that the study area may not be sheltered from relevant seismic sequences similar to the Mw 6 Emilia 2012 events and that the occurrence of potential seismogenic sources in the area should be carefully evaluated. Similar studies may be useful to constrain the present-day activity in other marine areas and to identify potential and hitherto unrecognized seismogenic sources along the entire Apennines belt and other accretionary prisms worldwide.

## 1. Introduction

Continuous GPS data analysis efficiently and routinely quantifies active deformation in seismically active areas of Italy and elsewhere (Bennett et al., 2012; Devoti et al., 2008; D'Agostino, 2014; Hammond et al., 2016; Kreemer et al., 2014), contributing to seismic risk assessment (Bird et al., 2010, 2015; Gualandi et al., 2017; Riguzzi et al., 2012). In contrast, the absence of available offshore seismic and CGPS data is reflected by a lesser knowledge of the tectonic activity in marine areas and, consequently, by a poor quantification of the seismic hazard affecting the nearby coastal areas. In Italy, one of those areas is the northern Adriatic Sea, where the lack of offshore CGPS data prevents from unequivocally constraining present-day deformation, leading to diverging opinions regarding the activity or inactivity of the most external thrusts of the Apennines belt (Argnani, 1998; Basili & Barba, 2007; Coward et al., 1999; Di Bucci & Mazzoli, 2002; Frepoli & Amato, 2000; Kastelic et al., 2013; Vannoli et al., 2004) (Figure 1). In particular, in the study area (see gray circle in Figure 2), the thrust front is located offshore. Available onshore geodetic data do not allow scientists to constrain the eventual occurrence of strong strain rate gradients, typical of actively deforming areas (e.g., Doglioni et al., 2015). As a consequence, despite the recognition of NE-verging thrust faults similar to those recognized in the adjacent sector of the frontal Apennines thrust belt and despite the instrumental (<http://terremoti.ingv.it/>) and historical (Rovida et al., 2020) seismicity, no seismogenic sources were so far hypothesized in the area focus of this study (Figure 2; Diss Working Group, 2018).

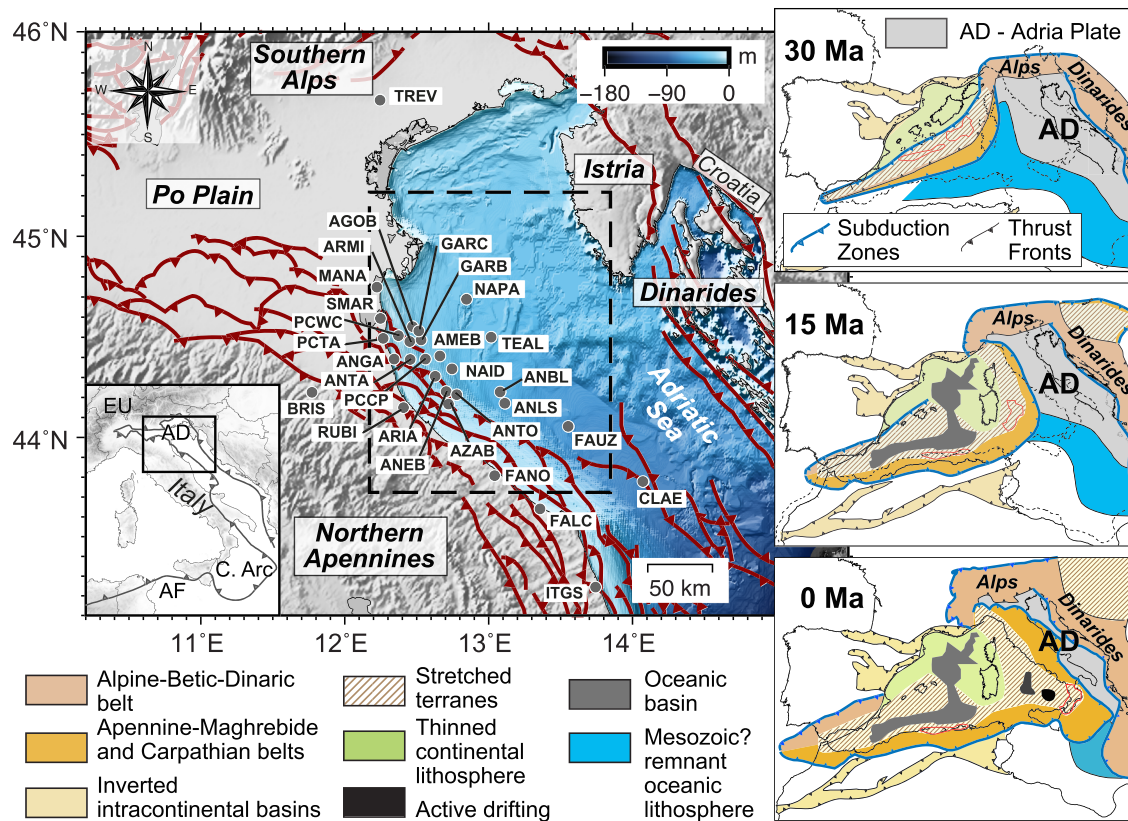


**Figure 1.** General setting of the study area and location of the CGPS stations (dark gray dots) in the northern Adria microplate (AD), within the structural framework proposed by Fantoni and Franciosi (2009) (dark red segments). High-resolution bathymetry of the Adriatic Sea is from the Emodnet database (<http://www.emodnet.eu/>). The dashed black box is the location of Figure 2. Inset: AF and EU stand for Africa and Eurasia plates, respectively, whereas C. Arc stands for Calabrian Arc. The 30, 15, and 0 Ma plate tectonics reconstructions are modified after Carminati et al. (2010). Dashed lines are the location of the present-day coastlines reported as a reference. The position and lateral extent of undeformed Adria are shown.

With the aim of filling this knowledge gap, we present an integrated study of geodetic and subsurface geological data from the northern Adriatic Sea (Figures 1–3). Analyses of available borehole and seismic reflection profiles are linked for the first time with CGPS data acquired on offshore hydrocarbon production platforms. These data were recently released by Eni S.p.A. company in the framework of “CLYPEA: Innovation network for future energy” Program, as part of the “Subsoil Deformations” Project (Antonucci et al., 2018, 2019). We also performed an analytical model in order to evaluate the control of main regional faults on the horizontal and vertical motions constrained by geodetic data. Although the influence of hydrocarbon production on the CGPS time series cannot be fully neglected, our results provide useful evidences to fill up the geodetic observational gap and provide an insight into the active thrust fronts offshore the northern Apennines. Similar multidisciplinary studies may prove to be useful also in other offshore thrust-fronts worldwide, where CGPS stations on hydrocarbon platforms are used mainly for monitoring the vertical seafloor motion related to hydrocarbon exploitation (Dacome et al., 2015; Haines et al., 2013), to define present-day deformation and possibly identify potential and hitherto unrecognized seismogenic sources.

## 2. Geological Setting

The tectonic evolution of the Africa-Eurasia convergent margin in the central Mediterranean has been deeply controlled by the inherited irregular geometry of the opposing plates and by the existence of Adria, a small continental plate that indented the Eurasian margins (Dewey et al., 1989; Doglioni, 1991; Malinverno & Ryan, 1986). The paleogeographic affinity of Adria and its kinematic relationship with major plates has been debated for decades. Adria microplate was interpreted either as a promontory of Africa

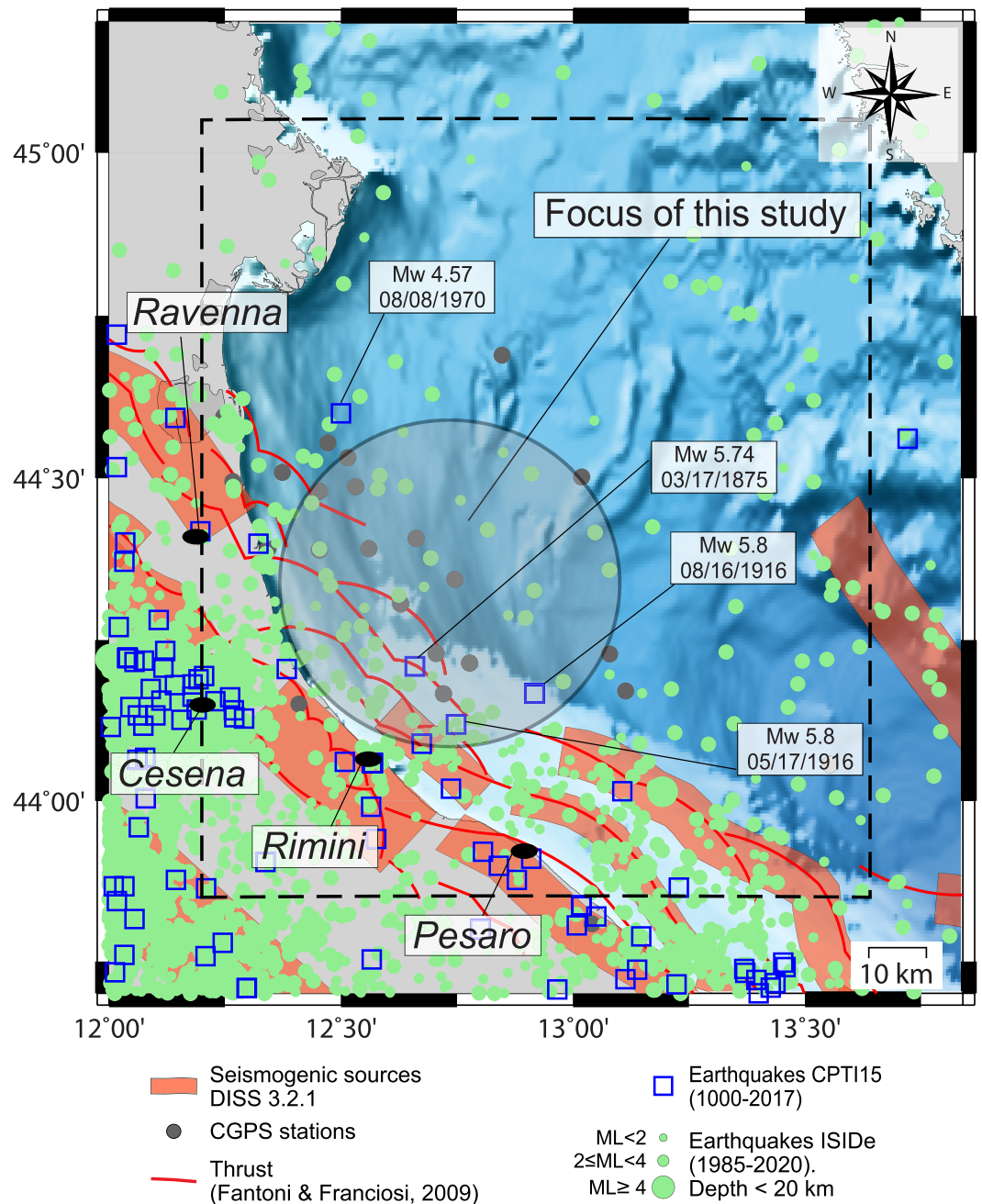


**Figure 2.** Potential seismicogenic sources (<http://diss.rm.ingv.it/diss/>), historical (<https://emidius.mi.ingv.it/>), and instrumental (<http://terremoti.ingv.it/>) seismicity of the northern Adriatic area with depth < 20 km. The historical earthquakes in the study area are reported. The dashed black box is the location of Figure 3a.

(Channell et al., 1979; Muttoni et al., 2001) or as an independent microplate (Battaglia et al., 2004; Dercourt et al., 1986). Since late Mesozoic time, the margins of Adria have been progressively involved in the ongoing deformation connected with the Africa-Eurasia convergence. Since Cretaceous time, the eastward subduction and the indentation of Adria have been decisive in the development of the W-verging Dinarides fold-thrust belt (Schmid et al., 2008). At that time, the northern portion of Adria became an active margin (Handy et al., 2010), owing to the E-SE-ward subduction of the ocean that separated Adria from Eurasia. Slices of Adria basement and cover (i.e., the Austro-Alpine nappes; Laubscher, 1989) overthrust the developing accretionary wedge toward the north. Compressional tectonics then moved to the south, with Paleocene-

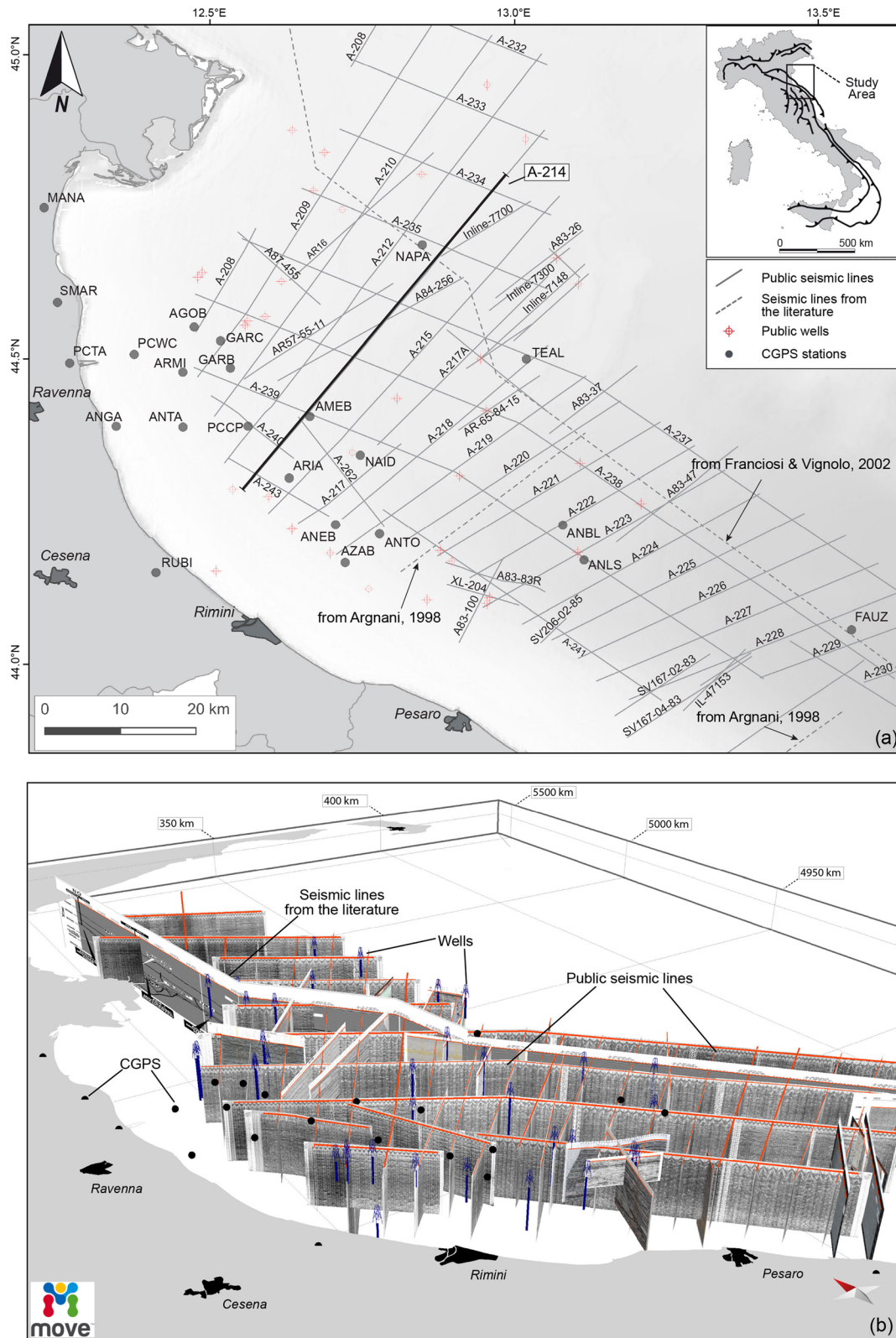


**Figure 3.** General view of subsurface data. (a) Location map of the data set used to reconstruct the subsurface structural framework of the northern Adriatic area. (b) 3-D view of the data set used for the reconstruction of the subsurface structural setting of the northern Adriatic area. Seismic reflection profiles, boreholes (in blue), and location of the CGPS stations (black dots) are shown. In the supporting information ([ftp://ftp.ingv.it/pub/giuseppe.pezzo/TECT\\_2020TC006425/](ftp://ftp.ingv.it/pub/giuseppe.pezzo/TECT_2020TC006425/)) we provide a dynamic 3-D view of the interpreted seismic profiles (Figure S1).

Holocene south-directed thrusting in the Southern Alps and Po Plain (Carminati et al., 1997; Roeder, 1989). To the west, the Adria margin began to be affected by compressional deformation in the Neogene time, with the onset and retreat of the W-directed Apennines subduction (Carminati et al., 2012; Patacca et al., 1990; Ricci Lucchi, 1986).

The undeformed part of the Adria plate shrank through time (Figure 1), consumed by the advancing trenches of the Apennines and Dinarides subduction zones and of the thrust front of the Southern Alps (Carminati et al., 2010). At present, part of Adria located below the Adriatic Sea and below the recent deposits of the Po Plain is still undeformed, whereas its margins have been involved in thrust tectonics associated with the Apennines, Dinarides, and Southern Alps orogens (see inset in Figure 1). Owing to this complex tectonic setting, the actual size of the Adria unaffected by compressional deformation (i.e., the foreland) is still debated. Geophysical investigations show that the opposite compressive fronts of the Dinarides and Apennines are almost in contact in the central Adriatic domain (Scisciani, 2009; Scrocca, 2006). Similarly, beneath the central and western Po Plain, the opposite Southern Alps and Apennines compressive fronts are almost in contact (Fantoni & Franciosi, 2010; Pieri & Groppi, 1981; Toscani et al., 2016; Turrini et al., 2015, 2016), with the Apennines thrust front characterized by an undulating geometry due to the development of salients and recesses controlled by lateral facies variations and/or the presence of regional strike slip faults (Castellarin & Vai, 1986; Costa, 2003; Cuffaro et al., 2010; Livani et al., 2018; Perotti, 1991).

Thus, the largest sector of the Adria foreland is located in the northern Adriatic Sea and in the eastern Po Plain (see Figure 1). Based on seismic exploration data analysis, the outermost Apennines thrust faults were identified in the northern Adriatic Sea beneath the synorogenic deposits dated Early Pliocene-Quaternary (Argnani, 1998; Bally, 1986; Bigi et al., 1992; Casero, 2004; Del Ben, 2002; Di Bucci & Mazzoli, 2002; Fantoni & Franciosi, 2009; Franciosi & Vignolo, 2002; Kastelic et al., 2013; Scrocca et al., 2007). Thrust fault geometry is controlled by two main detachment levels: a deeper one, located at the bottom of the Mesozoic-Paleogene sedimentary cover (within Triassic evaporites), and a shallower one, located in Early Miocene deposits (at the bottom of the Schlier Fm.) of the Neogene foredeep clastic succession (Barchi, 1998; Maesano et al., 2013; Massoli et al., 2006). Contractional structures are mainly represented by NE-verging and NW-SE-trending thrust-related anticlines (Argnani, 1998; Bally, 1986; Casero, 2004; Fantoni & Franciosi, 2009), strongly deforming the sedimentary succession up to the lower Pleistocene (Casero, 2004; Coward et al., 1999; Di Bucci & Mazzoli, 2002; Fantoni & Franciosi, 2009). In the northern area, in correspondence to the latitudes of Rimini and Ravenna, the most external (eastern or north-eastern) thrust front of the Apennines was proposed to be located 35 km offshore (Casero, 2004). Moving to the south, the interpretation of seismic-reflection data set (Bally, 1986; Maesano et al., 2013) allowed the identification of several blind thrusts with the most external thrust front located 30 km off Pesaro. Fault planes associated with these structures are deemed to be potential sources of moderate to large earthquakes in this region and are included in the DISS database (DISS Working Group, 2018; Figure 2). In our study area (i.e., offshore Cesena and Ravenna; gray circle in Figure 2), instrumental seismic catalog (<http://terremoti.ingv.it/>) shows seismic activity along the whole collision front. Historical seismic record (CPTI15v2.0; Rovida et al., 2020) reports earthquakes in both the proximity of our study area and the collisional front. An Mw 5.74 earthquake struck the Rimini offshore on 17 March and 16 August 1916 in the same area (Figure 2) damaging the city of Rimini and its surroundings (Camassi et al., 1991 and reference therein; Rovida et al., 2020). Furthermore, the historical catalog reports an Mw 4.57 earthquake on 8 August 1970 occurred in the northern sector of the Adriatic Sea (Molin et al., 2008; Rovida et al., 2020). However, owing to the incompleteness of historical records for offshore areas, the DISS database shows no potential seismogenic sources, which are instead present a few kilometers to the south and to the northwest. This gap makes our study relevant for many geoscientists, particularly those working on active tectonics and related hazards. Moreover, our study can contribute to identify potential lateral continuities between seismogenic sources, redefining fault planes dimensions, crucial for seismotectonics and hazard assessments.

### 3. Data and Methods

#### 3.1. Seismic Reflection Profiles and Borehole Composite Logs

To properly define the structural setting of the area, we used an integrated approach combining geological and geophysical data. Most data used in this work derive from the ViDEPI public database (<http://www.>

videpi.com), mainly consisting of 2-D seismic-reflection profiles from the “A” Italian commercial zone (northern Adriatic area), borehole composite logs, and structural maps in the time domain (Figure 3; seismic reflection profiles from the ViDEPI project organized in a 3-D environment by means of Move® software are available in the GFZ Data Services Repository: <http://doi.org/10.5880/figeo.2020.027>, Maffucci et al., 2020). Furthermore, we collected seismic profiles, structural geological maps, and geological profiles from Bally (1986), Argnani (1998), Franciosi and Vignolo (2002), Casero (2004), Finetti and Del Ben (2005), Fantoni and Franciosi (2009), Kastelic et al. (2013), Wrigley et al. (2015), and Amadori et al. (2019).

The quality of the seismic profiles is inhomogeneous as they were acquired across a wide time span (since about the 1960s to present) using different acquisition systems and parameters. The tracks of the geological and seismic profiles available both from the literature and the ViDEPI database were georeferenced and organized in a geographic information system (QGIS software, version 2.18.16). In particular, we georeferenced 88 seismic-reflection profiles and 35 borehole logs, which were then imported into a 3-D environment using the MOVE® software (Midland Valley, version 2016.2) that was used for the interpretation phase (Figure 3b). We used available time/depth charts for selected borehole logs, seismic interval velocities from the literature (Bally, 1986; Montone & Mariucci, 2015), and isochrone maps (<http://www.videpi.com>) to tie the seismic horizons. We interpreted and drew the following stratigraphic units (from top to bottom; Figures 4, 5, and S1 in the supporting information): the top of the Early Pleistocene (top Gelasian); the top of the Pliocene fore-deep succession; the pre-Pliocene unconformity (corresponding to the top of the Messinian Gessoso-Solifera Formation; Selli, 1973; Roveri et al., 2001) represented by a continuous reflector characterized by a high reflection coefficient; and, where recognizable, the top of the lower part of the Mesozoic carbonate multilayer (corresponding to the near top of the Marne a Fucoidi Fm.; Galluzzo & Santantonio, 2002 and reference therein). We also interpreted and drew the external front of the Apennines fold-and-thrust belt, that is, the envelope of the most external (eastward) contractional structures (Figure 4).

To elaborate an analytical model of fault-related deformation, we produced a geological cross section combining data from a depth-converted seismic profile, interpreted within this project (i.e., seismic line A-214; Figure 4) and a portion of a previously published geological cross section (cross section n. 5 in Fantoni & Franciosi, 2009) mainly located onshore (Figures 7 and 8). To depth-convert the A-214 seismic profile, we used the interval velocities extracted by Bally (1986) and Montone and Mariucci (2015).

### 3.2. CGPS Data

A wealth of CGPS stations is on duty in the onshore Peri-Adriatic area, not all providing standardized high-quality data. Both scientific and commercial institutions installed such networks several years ago for different purposes, and nowadays, these networks deliver, on a regular basis, raw GPS data to the public and scientific community. The majority of stations is located along the north-western border of the Adriatic plate. A combined velocity solution for the onshore CGPS stations was published by Devoti et al. (2017). In this work, in the aforementioned network, we include 31 onshore and offshore CGPS stations installed on onshore sites and on offshore hydrocarbon platforms of the Adriatic Sea. The platforms and related CGPS stations are operated by the Eni S.p.A. company (see Figure 1). A subset of available offshore CGPS time series was selected by Eni, excluding those that, due to hydrocarbon exploitation, largely deviate from the average regional tectonic motion. The raw data consist of CGPS observations sampled at 30 seconds, using high precision geodetic antennas mounted onboard of the offshore hydrocarbon platforms and onshore on deep-rooted concrete pillars. The CGPS data were processed by several processing centers in the framework of the CLYPEA project activities, each center producing highly precise geodetic solutions. Here we handled CGPS time series provided by the GAMIT and BERNESE processing software, whose solutions are both obtained from double differences of phase observables. All modeling parameters are consistent with the ITRF2008 standard, whose reference frame is established using at least 40 EUREF stations located on the Eurasian Plate. The Eni CGPS time series cover an overall time span of 19 years, from 1998 to 2017 (minimum 3.3 years and average 11.9 years). Details on modeling parameters, reference frame realization, and assessment of the obtained solutions are available at <https://doi.org/10.1594/PANGAEA.914358> (Palano et al., 2020).

We estimated linear velocities of both GAMIT and BERNESE solutions, together with the annual signal. Daily residuals with respect to the linear drift amount approximately to 5 and 2 mm in the vertical and

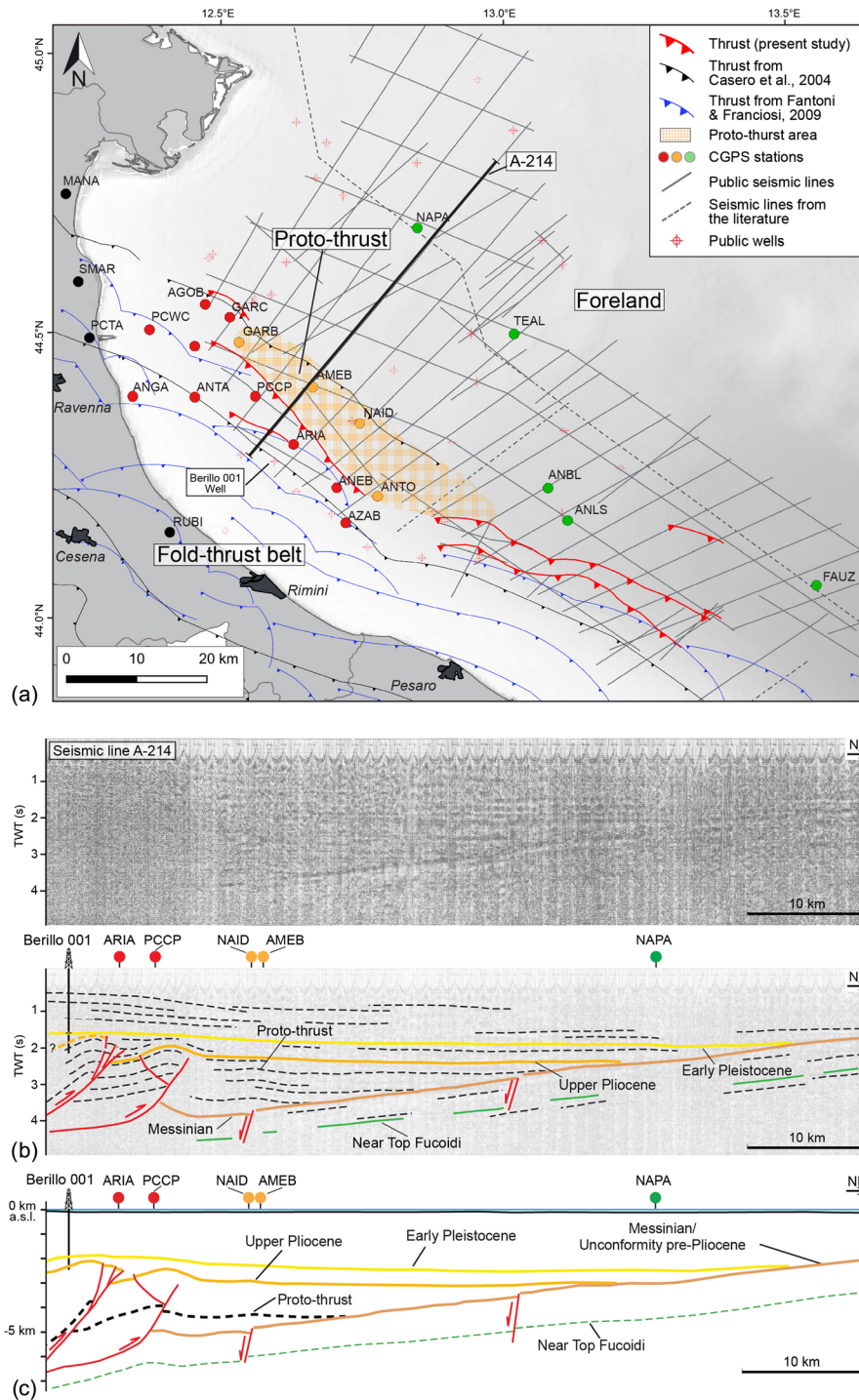


**Figure 4.** Results of the seismic profile interpretation. (a) Schematic structural map of the study area with the main tectonic domains recognized in the present work, that is, from west to east: fold-thrust belt, proto-thrust domain, and foreland, where the proto-thrust is the transitional domain between the fold-thrust belt and the foreland. Thrust traces from previous works (see text for references) are also drawn for comparison. The CGPS stations are distinguished with different colors according to the related tectonic domain: red for the fold-thrust belt, orange for the proto-thrust domain, and green for the undeformed foreland domain. The thick black line shows the location of the A-214 seismic profile and its depth-converted geological section shown in panels b and c, respectively. (b) A-214 seismic profile uninterpreted (above) and interpreted (below). The CGPS stations close to the seismic profile are perpendicularly projected onto the profile and distinguished with different colors according to the related tectonic domain (red, orange, and green for fold-thrust belt, proto-thrust, and foreland domain, respectively). In this seismic profile, the following major structural features can be recognized: the fold-thrust belt (west), the undeformed foreland (east), and the slightly deformed proto-thrust domain between the fold-thrust belt and the foreland. (c) Geological section after depth conversion of the A-214 seismic profile. Vertical exaggeration = 2.

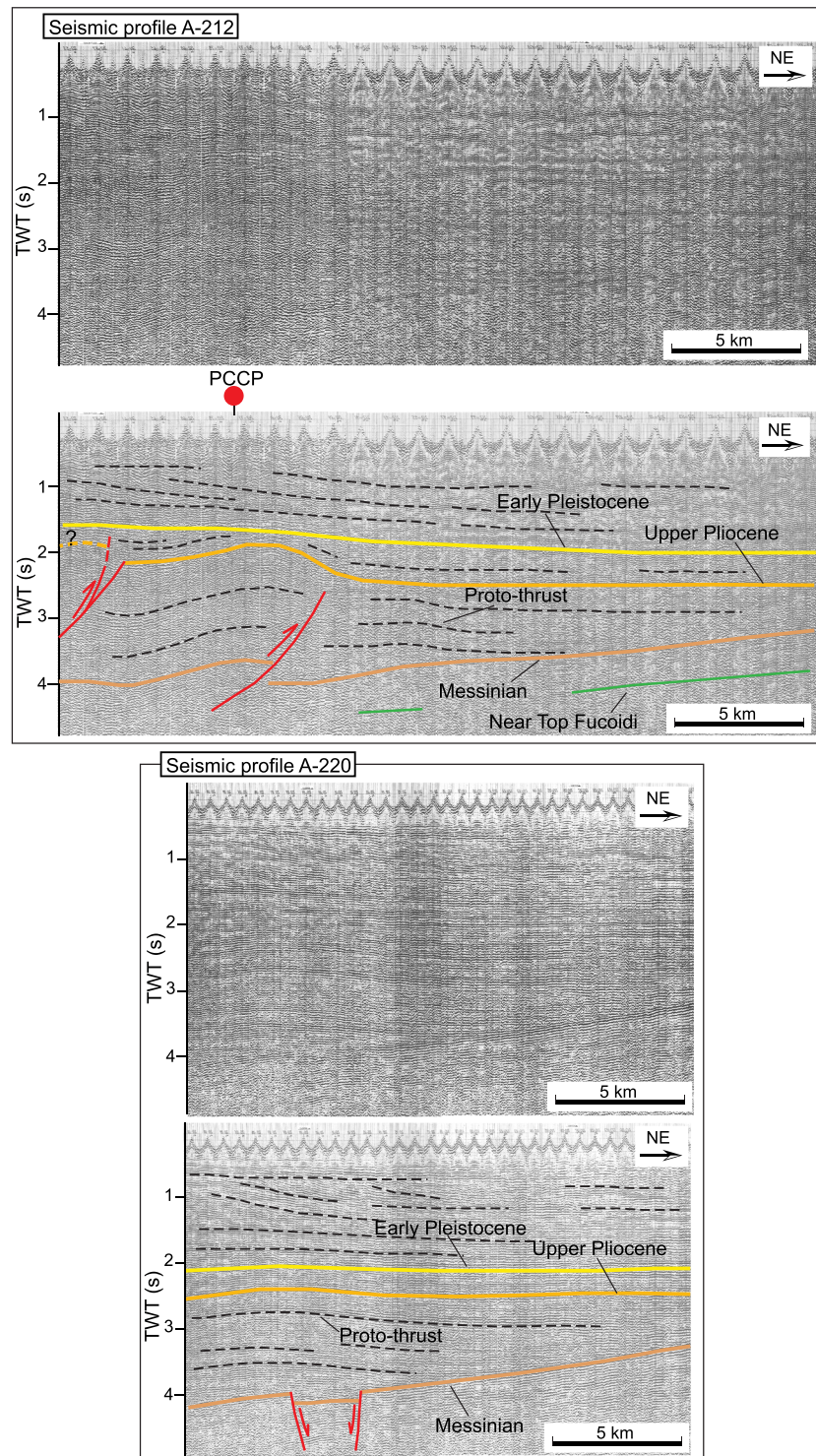


**Figure 5.** Uninterpreted and interpreted versions of the western part of two seismic reflection profiles. Location is shown in Figure 3. Pliocene slightly folded horizons belonging to the proto-thrust domain are well visible in both profiles. They are localized between the compressional structures of the fold-thrust belt domain to the west and the undeformed foreland to the east (seismic profile A-212). The foreland monocline, gently dipping toward the west, is affected by several normal faults dissecting the Miocene deposits and sutured by the Plio-Pleistocene deposits (seismic profile A-220).



horizontal directions, respectively, after filtering for the annual signal. We combined the two velocity solutions into a unified velocity field, following the velocity combination strategy adopted by Devoti et al. (2017). Differences between the combined velocity and the BERNESE and GAMIT velocity fields are at the level of 0.2 mm/yr (Weighted-Root-Mean-Squared, WRMS) that are consistent with the average velocity standard deviation of 0.3 mm/yr. To include the regional velocity field of Devoti et al. (2017), we rotated and scaled the combined velocity solution on the regional velocity field, thus including the offshore velocities in the same regional reference frame. To express the velocity field with respect to the Adria plate, we selected 21 CGPS stations representative of the Adria undeformed rigid plate and estimated the relevant Eulerian pole (see supporting information for details at [ftp://ftp.ingv.it/pub/giuseppe.pezzo/TECT\\_2020TC006425/](ftp://ftp.ingv.it/pub/giuseppe.pezzo/TECT_2020TC006425/)). The complete CGPS velocity field given in the Adria-fixed frame is shown in Figure 6.

At the time scale of a few years, Adria plate kinematics can be considered as a stationary process (Anderlini et al., 2020; D'agostino et al., 2005, 2008; Devoti et al., 2008). Therefore, we consider the linear velocity model as the most suitable description of the tectonic displacement at the CGPS points; however, the offshore platforms may be affected by local ground deformation due to the exploitation of gas fields, and CGPS velocities may thus vary with time. Depending on the hydrocarbon production rate as well as on the geometry, depth, and geological setting of the reservoir, CGPS receivers may measure subsidence and, to a lesser extent, horizontal non-tectonic displacements correlated with hydrocarbon production (i.e., reservoir depletion). Unfortunately, daily well production parameters are currently not freely accessible. The available production data quantify the cumulated monthly production of the entire reservoir, thus referring to several platforms. Moreover, offshore platform CGPS time series systematically started after the onset of reservoir production, making it difficult to discriminate anthropic contributions from the natural ones and impeding any modeling attempt. We, instead, used a nonlinearity indicator to quantify the deviation from the linear behavior of the tectonic signal. The nonlinearity index ( $I_{NL}$ ) corresponds to the ratio between the standard deviation of the smoothed time series and the standard deviation of its intrinsic noise:

$$I_{NL} = \frac{\sqrt{\sum_{i=1}^N |F_i - \bar{F}|}}{\sqrt{\sum_{i=1}^N |R_i - \bar{R}|}}$$

where  $i = 1 \dots N$  is the number of data and  $F$  and  $R$  (with mean values  $\bar{F}$  and  $\bar{R}$ ) are the smoothed and the residual observations, respectively.

An estimate of the intrinsic noise may be achieved by computing the standard deviation of residuals with respect to a smoothed curve that approximates the low frequency behavior. We smoothed the time series using a moving average filter with a sliding window of 1 year, so that the residuals will contain most of the high frequency noise.  $I_{NL}$  values  $\leq 0.5$  reflect time series with pure linear behavior and will increase as the time series deviate from any linear trend. Consequently, assuming the tectonic process as linear in our observable time windows, for subsequent tectonic modeling we consider three quality classes (A, B, and C) for CGPS time series with  $I_{NL} \leq 0.5$ ,  $0.5 < I_{NL} \leq 1.0$ , and  $I_{NL} > 1.0$ , respectively (Table 1 reports the  $I_{NL}$  values of each time series and of each component).

### 3.3. Modeling of Fault-Related Deformation

In order to estimate the current slip rate of the major identified faults, we simulated the surface deformation associated with an uniform slip over the regional thrust detachment, by using a simple 2-D modeling approach, largely applied to different tectonic domains worldwide (e.g., Anderlini et al., 2020; Fialko, 2006; Pezzo et al., 2012; Ponraj et al., 2019; Vergne et al., 2001). The computation of a 2-D profile model allowed us to simulate an infinite wide (perpendicular to the profile) regional thrust detachment, avoiding lateral deformation effects (Figure 6). The approach adopts Okada's (1985) formalism and allows to predict the surface displacements due to the slip of a fault plane embedded in an isotropic elastic half-space. We assumed an isotropic elastic Poisson solid for the crustal half-space with Young's Modulus of  $8 \times 10^5$  bars and Poisson's ratio of 0.25. We used the COULOMB software (Toda et al., 2011), which calculates shear and normal components of the static stress change and associated vertical and horizontal displacements on a 3-D grid, caused by the prescribed slip along a fault. The geometry of the modeled thrust fault is based on the depth-converted seismic profile of Figure 4 (A-214 seismic profile) integrated with a regional



**Table 1**  
*Kinematic and Tectonic Attributes and Location of the CGPS Stations in the Northern Adriatic Area*

Station	Lon.	Lat.	Height	E Vel.	N Vel.	H Vel.	E I <sub>NL</sub>	N I <sub>NL</sub>	H I <sub>NL</sub>	AT I <sub>NL</sub>	I <sub>NL</sub> class	Time span	Tectonic setting	Seismic profiles
	(deg)	(deg)	m	mm/y	mm/y	mm/y	-	-	-	-	A,B,C	(y)		
AGOB	12.47	44.55	67	1.0 ± 0.1	-1.0 ± 0.1	-7.5 ± 0.2	0.41	0.61	0.74	0.51	B	14.2	P-T	A208
AMEB	12.66	44.41	73	-1.0 ± 0.1	-0.5 ± 0.1	-2.3 ± 0.4	0.55	0.19	0.45	0.37	B	19.1	P-T	A214, A239
ANBL	13.08	44.23	77	0.1 ± 0.1	0.7 ± 0.2	-4.0 ± 0.3	0.61	0.71	0.90	0.66	B	10.4	F	A222
ANEB	12.70	44.23	64	-1.0 ± 0.1	-0.2 ± 0.1	-4.4 ± 0.3	0.34	0.97	0.36	0.66	C	10.4	F-T	A218
ANGA	12.34	44.39	73	0.5 ± 0.1	1.8 ± 0.1	-16.8 ± 0.3	1.09	1.04	1.61	1.07	C	19.1	F-T	...
ANLS	13.11	44.17	63	-0.9 ± 0.1	0.3 ± 0.1	-4.4 ± 0.4	0.51	0.30	0.66	0.41	B	10.2	F	A223/A239
ANTA	12.45	44.39	73	-0.9 ± 0.1	0.4 ± 0.1	-5.4 ± 0.3	0.76	0.54	0.79	0.65	B	12.0	F-T	...
ANTO	12.78	44.21	68	-0.7 ± 0.1	0.7 ± 0.1	-2.6 ± 0.3	0.39	0.46	0.33	0.43	A	10.4	P-T	A219
ARIA	12.63	44.31	69	1.3 ± 0.1	0.3 ± 0.1	-10.9 ± 0.3	0.35	1.15	0.70	0.75	C	13.6	F-T	A215
ARMI	12.45	44.48	73	0.2 ± 0.1	0.02 ± 0.1	-4.9 ± 0.4	0.53	0.40	0.40	0.47	A	9.1	F-T	A209
AZAB	12.72	44.17	78	0.2 ± 0.1	0.8 ± 0.1	-4.0 ± 0.3	0.33	0.34	0.49	0.34	A	12.5	F-T	A219
CERA	12.64	44.29	68	0.8 ± 0.1	0.6 ± 0.1	-11.9 ± 0.2	0.72	2.48	0.50	1.60	C	14.2	-	...
CLAE	14.07	43.78	66	-1.3 ± 0.1	-2.3 ± 0.1	-14.7 ± 0.4	1.30	1.82	0.37	1.56	C	10.0	F-T	...
ELEO	14.16	42.84	73	0.04 ± 0.3	-0.1 ± 0.5	-0.3 ± 1.0	0.24	0.32	0.17	0.28	A	5.0	F-T	...
EMIL	14.24	42.93	66	-0.3 ± 0.2	0.0 ± 0.4	-2.8 ± 0.5	0.34	0.30	0.28	0.32	A	8.8	F-T	...
FALC	13.36	43.64	46	0.5 ± 0.1	0.8 ± 0.2	-0.7 ± 0.3	0.29	0.36	0.26	0.33	A	10.1	F-T	...
FANO	13.04	43.81	51	0.1 ± 0.1	1.1 ± 0.1	-0.2 ± 0.3	0.48	0.54	0.28	0.51	B	10.1	F-T	...
FAUZ	13.55	44.06	67	-1.4 ± 0.4	1.4 ± 0.5	-7.1 ± 1.6	0.24	0.10	0.32	0.17	A	3.3	F	A228/A229/ A238
FIUN	12.53	44.40	44	7.0 ± 0.1	-2.1 ± 0.1	-14.5 ± 0.2	3.11	1.44	1.26	2.28	C	15.8	-	...
GARB	12.53	44.49	66	-0.8 ± 0.1	0.0 ± 0.1	-7.0 ± 0.3	0.71	0.59	0.82	0.65	B	14.2	P-T	A209/A210
GARC	12.52	44.53	73	-1.6 ± 0.1	-0.1 ± 0.1	-7.8 ± 0.3	0.52	0.58	0.67	0.55	B	14.2	P-T	A209
MANA	12.23	44.75	44	0.2 ± 0.1	-0.2 ± 0.1	-3.3 ± 0.3	0.55	0.52	0.26	0.54	B	12.5	...	...
NAID	12.75	44.34	62	-1.4 ± 0.1	-0.1 ± 0.1	-3.8 ± 0.3	0.45	0.40	0.53	0.43	B	12.5	P-T	A215/A217
NAPA	12.85	44.69	69	0.0 ± 0.1	-0.3 ± 0.1	-2.6 ± 0.3	0.72	0.40	0.29	0.56	B	15.5	F	A235, A212/ A214
PCCP	12.56	44.39	72	1.5 ± 0.1	-0.9 ± 0.1	-4.5 ± 0.3	0.46	0.42	0.40	0.44	A	12.5	F-T	A212, A240
PCTA	12.27	44.49	45	2.2 ± 0.1	2.2 ± 0.1	-7.5 ± 0.3	1.08	1.16	0.79	1.12	C	15.7	F-T	...
PCWC	12.37	44.51	72	0.5 ± 0.1	-0.5 ± 0.1	-4.9 ± 0.3	0.34	0.36	0.77	0.35	B	14.7	F-T	...
RUBI	12.41	44.15	47	0.2 ± 0.1	1.7 ± 0.1	-2.6 ± 0.3	0.54	0.48	0.69	0.51	B	10.1	F-T	...
SMAR	12.25	44.59	44	-0.6 ± 0.1	0.3 ± 0.1	-6.4 ± 0.3	0.45	0.28	0.60	0.37	B	15.7	F-T	...
TEAL	13.02	44.50	66	-1.7 ± 0.1	0.6 ± 0.2	-4.8 ± 0.3	1.10	1.14	0.71	1.12	C	10.1	F	A218/A237
TREV	12.25	45.67	70	-0.4 ± 0.1	-0.4 ± 0.2	-0.7 ± 0.3	0.29	0.26	0.23	0.28	A	10.0	-	...

*Note.* Abbreviations of tectonic settings are as follows: P-T, proto-thrust; F, foreland; F-T, fold-thrust belt. The “Height” column indicates the GPS vertical positions above the WGS84 ellipsoid; E, N, H, and AT I<sub>NL</sub> represent the nonlinearity indexes of the eastern, northern, vertical, and along track directions, respectively.

profile published by Fantoni and Franciosi (2009; see their cross section no. 5). Based on the reconstructed subsurface geology, we calculated the ground displacement velocity profile (Figures 7 and 8) assuming a uniform slip rate along the basal detachment thrust fault (dipping 6° toward the west, with the top tip point at a depth of 5.6 km and the bottom tip point at 11 km) (Figures 7 and 8). For this thrust front portion, Maesano et al. (2015) evaluated slip rates varying from 0.11 to 2.23 mm/yr distributed along different structures (thrust and back thrust) in different time interval (since 3.6 Myr). In our simple model, we explored current aseismic slip rate in a range from 0.1 up to 3.5 mm/yr occurring along a weak portion of the detachment, whereas its upper portion is forced to be locked (Figures 7b and 8b). However, models characterized by slip rate <1.5 mm/yr or >2.5 mm/yr are not able to fit the observed ones (see Figure S2). On the other hand, models taking into account slip rate values ranging between 1.5 and 2.5 mm/yr show velocity profiles compatible with CGPS observations.

## 4. Results

### 4.1. Subsurface Geology

The interpretation of the seismic profiles (see supplemental material in the external repository at <http://doi.org/10.5880/fidgeo.2020.027> (Maffucci et al., 2020) allowed us to reconstruct the structural framework of the northern Adriatic domain and to define the tectonic setting where the CGPS stations are located (Figures 1–

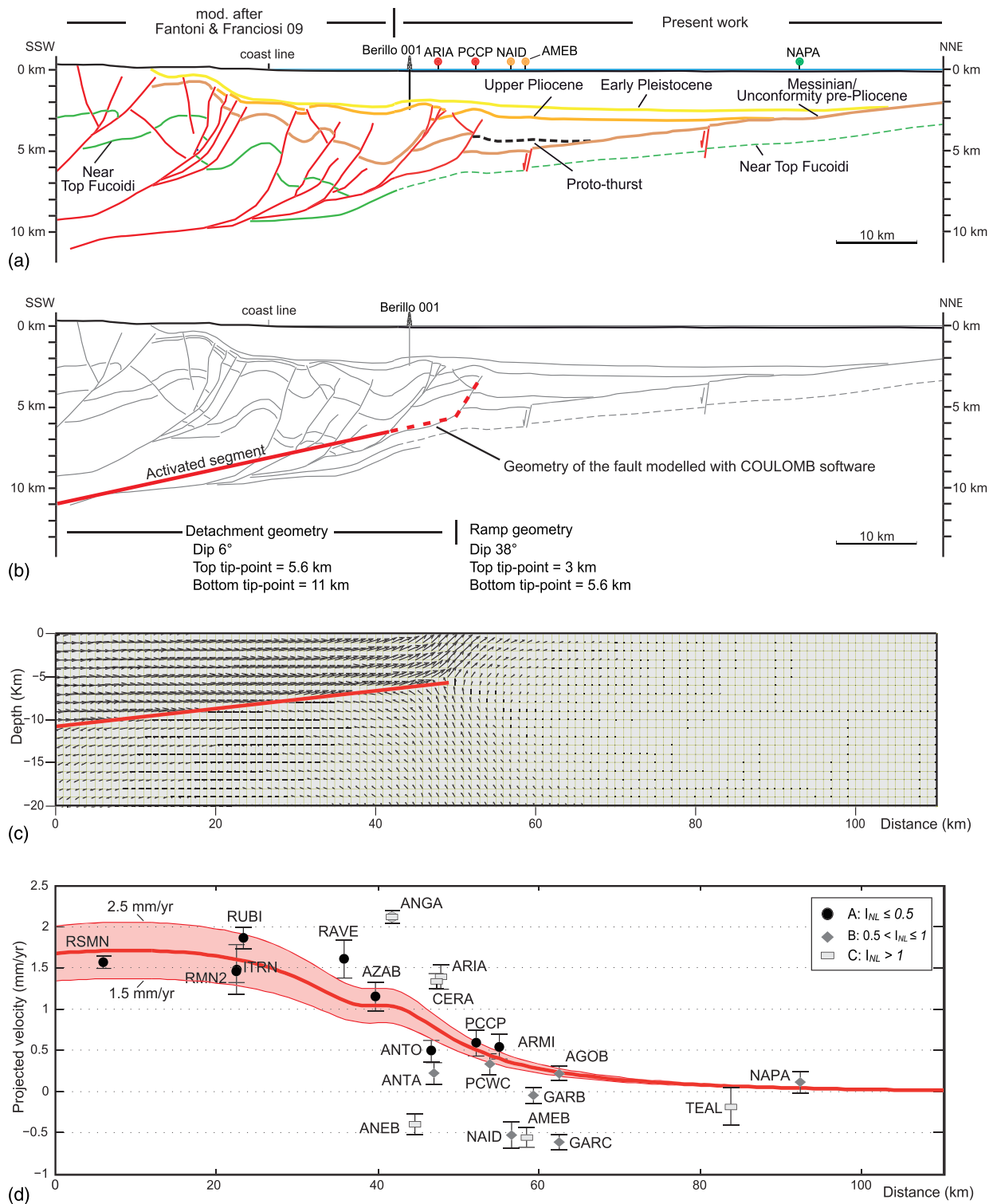


**Figure 7.** Horizontal CGPS velocities and modeling results along a geological profile. (a) Geological cross section along the profile trace shown in Figure 4 obtained merging the cross section of Figure 4c and the cross section no. 5 in Fantoni and Franciosi (2009). Vertical exaggeration = 2. (b) Geometry in section view of the fault modeled with COULOMB software. The solid red line represents the portion of the detachment activated. Vertical exaggeration = 2. (c) Modeled cross section velocity vectors along the geological transect as shown in panel (a) and (b); no vertical exaggeration is applied. (d) Horizontal observed CGPS (black to gray dots) and modeled velocities (red line) projected along the same profile of (a). The CGPS stations have been classified according to their nonlinearity indicator to quantify the deviation from the linear behavior of the tectonic signal;  $I_{NL}$  values  $\leq 0.5$  reflect time series with pure linear behavior. The red band represents the horizontal velocities estimated from models taking into account slip rate values in the 1.5–2.5 mm/yr interval (see the text for details).



3). The study area is characterized by compressional structures to the west, represented by thrust faults and related folds in their hangingwall, and by the undeformed foreland to the east (Figures 4 and 5). The foreland monocline gently dips toward the west as shown by the visible inclined reflector of the pre-Pliocene unconformity, which is recognizable in all the investigated seismic profiles. The foreland monocline is affected by a series of extensional faults (Figures 4b and 4c and A-220 seismic profile in Figure 5) confined within the pre-Messinian deposits and upward sutured by the Plio-Pleistocene deposits. A reconstruction of the main thrust front (Figure 4a) is obtained by the interpolation in a 3-D environment of closely spaced seismic profiles (Maffucci et al., 2020). In particular, we reconstructed two external NW-SE-trending thrust planes (Figure 4a). According to the cross-cutting relationships between seismic-reconstructed horizons and thrusts, the tectonic activity occurred since (at least) Gelasian time. Due to low resolution of seismic data, particularly in the shallow portion of the seismic profiles, we are not able to establish with confidence (only with the structural interpretation) whether the tectonic activity lasted until recent-present times.

A particular feature that we observed along several seismic profiles in the northern portion of the study area is the occurrence, to the east of the most external (the easternmost one) thrust, of Pliocene slightly folded seismic horizons (Figures 4b, 4c, and 5). Figure 4 shows one of the most interesting seismic profiles highlighting all the structural features of the area. In this seismic profile, we identified two blind thrusts with a minor splay to the west and the flexure of the pre-Messinian sedimentary sequence dipping toward the west. Furthermore, we observed the folded sector in front (east) of the external thrusts, which involve Pliocene sediments and are detached along the Messinian deposits. Based on the aforementioned seismic-reflection evidence, we identified three different tectonic domains (from west to east): the fold-thrust belt, the proto-thrust domain, and the undeformed foreland. The CGPS stations studied in this paper are distributed over these three tectonic domains and are shown in detail in Figure 4 (Table 1).

#### 4.2. CGPS Velocities Compared to Analytical Models

Observed and modeled horizontal velocities are characterized by curved positive (moving toward NE) values along the onshore portion of the profile (between 0 and 40 km). From the 40th to 70th km along the profile, velocities steeply decrease down to zero, associated with the Apennines-Adria compression. From the 70th km to the end of the profile (east), velocities are almost null, indicating negligible deformation. The modeled velocity profile fits well the class A ( $I_{NL} \leq 0.5$ ) CGPs stations velocities. Data fit decreases with increasing  $I_{NL}$ , as observable for class B ( $0.5 < I_{NL} \leq 1.0$ ) and C ( $1.0 < I_{NL}$ ) stations, highlighting how tectonic velocity models well reproduce present-day linear velocities and promoting the  $I_{NL}$  as a good indicator of the data reliability for tectonic studies. The slip rate along the basal detachment thrust fault is not fully constrained because of the large scattering in the CGPS velocities, and we can only take into account values from 1.5 to 2.5 mm/yr (Figures 7 and 8). Into this window of slip rate values, we are not able to favor for a single model, and the best fitting value of 2 mm/yr should be considered approximate.

Modeled vertical velocities indicate negligible values along the entire profile, with a small gentle bulge (about 1 mm/yr) between the 30th and 60th km along the profile. On the contrary, observed velocities show an important subsidence pattern covering a large portion of the profile. Higher vertical velocities are observed for the class C stations, characterized by higher nonlinearities in the time series, highlighting the nonlinear behavior of the anthropogenic signal in geodetic records.

### 5. Discussions

The external fronts of the Apennines fold-thrust belt are characterized by NE-verging blind thrusts, which cut and deform the sedimentary succession up to at least the Gelasian deposits (Figures 4, 5, 7, and 8). Our interpretation of the seismic profiles is coherent with previous works (Argnani, 1998; Bally, 1986; Bigi et al., 1992; Casero, 2004; Del Ben, 2002; Di Bucci & Mazzoli, 2002; Fantoni & Franciosi, 2009; Franciosi & Vignolo, 2002; Kastelic et al., 2013; Scrocca et al., 2007); however, the proposed position of the frontal thrusts is slightly different from that of previous works (Casero, 2004; Fantoni & Franciosi, 2009). In the study area, considering the spacing between the seismic profiles, the external fronts (except for two isolated small thrusts) are apparently continuous, reaching 40 km in length, and oriented nearly parallel to the coastline. The central portion of the study area (close to the AZAB CGPS station in Figure 4) is characterized by a gap of the seismic profiles (except for one seismic line from the literature;

Argnani, 1998), and it is not possible to properly define the position of the frontal thrusts. Moving toward the foreland, in the footwall of the most external thrust fault, Pliocene sediments are slightly folded in a rather continuous sector, interpreted as a proto-thrust zone (Gulick et al., 2004; Moore et al., 1995, 2005), between the foreland to the east and the fold-thrust belt to the west (Figures 4 and 5). The foreland is gently dipping toward W-SW, and it is cut by normal faults sealed by Pliocene sediments because of the foreland bulging.

Interpreting seismic profiles, some authors suggested that shortening along the external front of the Apennines chain in the central and northern Adriatic Sea ceased between middle Pliocene and the early Pleistocene time (e.g., Argnani, 1998; Coward et al., 1999; Di Bucci & Mazzoli, 2002), whereas others, coupling seismological, geophysical, and geological analyses, concluded that shortening, possibly accommodated by seismogenic faults, may still be active nowadays (Basili & Barba, 2007; Frepoli & Amato, 2000; Kastelic et al., 2013; Montone & Mariucci, 2016; Vannoli et al., 2004). In summary, although in recent years evidences for active tectonics along this part of the Apennines thrust front seem to prevail, no smoking guns have been found. Based on previously discussed offshore CGPS data, the active/inactive nature of thrust fronts will be addressed in the following.

The velocity vectors calculated for the CGPS stations in the Po Plain represent the stable ADRIA plate motion (red arrows in Figure 6). Deformation becomes progressively compressional in the Apennines fold and thrust belt, as highlighted by the sharp velocity gradients (black arrows in Figure 6). The WRMS of the horizontal velocities of the Adria plate is in the order of 0.25 mm/yr, which represents the noise level of the velocity field in this representation. As expected, the offshore velocity vectors are less coherent than the onshore ones because of their intrinsic nonlinear behavior connected with non-tectonic processes. For this reason, we used the  $I_{NL}$  that rapidly allowed us to classify CGPS based on their nonlinear behaviors of the corresponding time series. By projecting the horizontal velocities along a transect across the fold-thrust belt toward the Adriatic Sea (Figure 7), we observe that class B and C stations (higher  $I_{NL}$ ) are badly fitted by the tectonic model and show stronger subsidence patterns, likely due to hydrocarbon production activities (Figure 8). On the contrary, our tectonic model well reproduces the class A stations (lower  $I_{NL}$ ) velocities. CGPS data indicate a decrease of velocities associated with active shortening between the 40th and the 70th km along the profile of Figure 7 (active contraction in the frontal part of the Apennines toward the east) and negligible velocities from the 70th km to the end of the profile (Adriatic foreland). This velocity gradient clearly indicates the eastward transition from active thrust faults to proto-thrusts (i.e., incipient thrusting/shortening) and undeformed foreland areas (Figure 9).

The shape of the observed CGPS horizontal velocity profile mirrors that predicted by our model (Figure 7d). This means that, in the regional analysis that we are addressing, most of the movement highlighted by CGPS data can be explained by the slip along the basal detachment surface and that the effect of the slip along the ramp is rather negligible. Based on this analysis, we hypothesize that some (mainly aseismic) slip along the detachment fault may explain the current horizontal velocity field in the northern Adriatic region. Such slip activated, in the geological past, the ramp at the thrust front, probably with a stick-slip behavior, whereas it produced only folding and fracturing in the proto-thrust area. At present, the frontal thrust ramp is locked, as indicated by the described steep horizontal velocity gradient. We speculate that the ongoing slip along the detachment might elastically load the locked ramp at the thrust front, which may possibly fail and seismically slip, although no inferences can be made on the timing. Coupling our reconstruction of the geological structures geometry with the CGPS data analysis and modeling, we propose that deformation of the external Apennines fold-thrust belt is presently active, in agreement with some previous works (e.g., Basili & Barba, 2007; Kastelic et al., 2013; Vannoli et al., 2004), extending the active external front of the Apennines chain also in this sector of the Adriatic Sea. In this view, the outermost ramp of the northern Apennines belt in the studied marine region may be a potential seismic source, although other more internal thrust faults could be potentially seismic as well. Considering the detachment depth (Petricca et al., 2019), we cannot exclude, along these structures, seismic events, similar to the Mw 6.0 and Mw 5.8 2012 Emilia earthquakes (e.g., Govoni et al., 2014; Pezzo et al., 2013, 2018) and to those reported in the historical seismic catalog (e.g., Camassi et al., 1991 and references therein; Molin et al., 2008), even though seismic reflection profiles in our and previous studies (Di Bucci & Mazzoli, 2002 and references therein) show no evidence of active tectonic deformations. This lack of evidences in the recent Quaternary deposits could be related to the effect of the large increase of sediment supply in the foredeep during the Quaternary eustatic low stand, which eventually produced a smaller apparent fault throw or masked the internal tectonic deformation

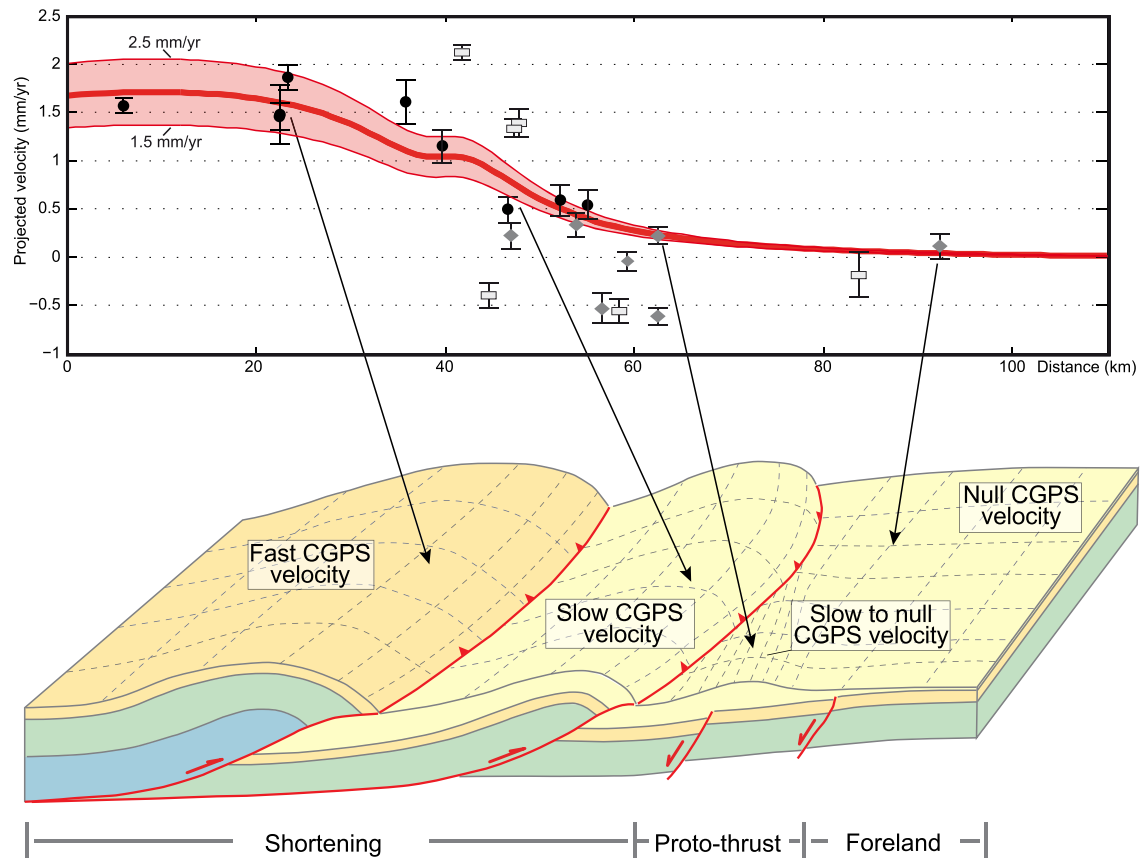


**Figure 9.** Conceptual sketch. 3-D conceptual sketch showing the relationship between the CGPS velocities, the surface deformation from the numerical model, and the geological structures.

(Scrocca et al., 2007). Indeed, Doglioni and Prosser (1997) highlight the interplay between regional foredeep subsidence, anticlines uplift rate and sedimentation rate in the study area, where regional subsidence is higher than anticlines uplift rates and sediments fill this space. Furthermore, it is worth mentioning that blind thrusts are typical in regions characterized by slow convergence rates (Petricca et al., 2018), like those observed in the study area. In this case, fault propagation at depth is possibly associated with a fault propagation fold (Suppe & Medwedeff, 1990), showing an exiguous folding of the shallow sediments and without any brittle deformation at surface (no evidence of capable faults; Petricca et al., 2018).

Concerning the vertical component, CGPS data show strong subsidence, up to 10–15 mm/yr (Figure 6b and Table 1). Modeled velocities do not fit the observed ones (Figure 8d), indicating that aseismic tectonic slip along the detachment fault is not the main process controlling vertical displacements in this area, even at the class A stations ( $I_{NL} \leq 0.5$ ) that measure vertical velocities < 5 mm/yr and, as previously evidenced, are less prone to anthropic displacement signals.

Although on long-term spans, the effects of earthquakes on the vertical deformation patterns cannot be ruled out (Carminati et al., 2007), a significant amount of the natural subsidence in this region is related to the active flexure of the Adriatic plate associated with the northeastward retreat of the Adriatic subduction (Carminati et al., 2005). The asymmetry of the Apennine foredeep implies subsidence rates up to 10 times higher with respect to the Alpine and Dinaric ones (Doglioni, 1993; Mariotti & Doglioni, 2000). Moreover, sediment load/compaction and deglaciation-related ice melting also contribute to the subsidence, resulting in a total (along coast) natural subsidence rate of about 3 mm/yr (Carminati et al., 2003). This value is expected to decrease significantly moving offshore, toward the foreland of the Apennines, where the Adriatic plate flexure is expected to reduce significantly. Unfortunately, this pattern cannot be exactly quantified due to the current lack of reliable data; however, by analogy with what occurs along a transect from the



Apennines to the foreland across the Po Plain (Cuffaro et al., 2010), we expect a natural subsidence decrease of 2 mm/yr in the offshore, at a distance of 100 km from the coast. With the exception of a few offshore GCPS stations in the area (ITRN, RMN2, ROBI, ANTO, AMEB, and NAPA), the other stations indicate subsidence rates largely exceeding these natural subsidence rates. For these stations, other causes for subsidence need to be investigated, such as anthropic activities.

## 6. Conclusions

In the northern Adriatic Sea, the interpretation of subsurface geological and CGPS data allowed us to identify the previously unrecognized kinematically active transition from the Apennines fold-thrust belt, to the west, to the Adriatic foreland, to the east. In particular, based on geodetic and subsurface geological data analysis, modeling, and interpretation, we detected the Apennines-Adriatic foreland transition along a NW-SE oriented 30 km wide zone where the CGPS velocities gradient allows us to constrain a shortening of 1.5 mm/yr. Toward the east, this transition involves a fold-thrust domain moving eastward at 1.5 mm/yr. The frontal thrusts fade away into a region of proto-thrusts (incipient thrusting) moving eastward at 0.5 mm/yr, gradually decreasing down to zero into the undeformed Adriatic foreland. Our 2-D analytical models across the thrust front well reproduce the observed velocity profile, estimating a slip rate between 1.5 and 2.5 mm/yr. Concerning vertical velocities, the observed subsiding pattern can be partly explained by the Adria subduction-related subsidence in the foredeep basin and partly by anthropic activities such as hydrocarbon exploitation, which must be further studied to be fully understood.

Offshore geodetic data coupled with seismic reflection and geological data provided new insights into the active tectonics and contribute to define the current activity of the thrust front area, currently accommodated by aseismic slip along the basal detachment, likely accumulating elastic energy along its upper portion and the frontal ramp, which may eventually slip seismically. However, although seismic activity characterizes this offshore sector of the Apennines fold-thrust belt, no potential seismic sources are considered in published databases.

For these reasons, we conclude that the studied portion of the external front of the Apennines fold-thrust belt in the northern sector of the Adriatic Sea is still active. Despite the fact that the incompleteness of historic seismic catalog prevents a clear identification of potential seismogenic sources, our results suggest that the study area may not be sheltered from relevant seismic events and, although further work is needed to assess its seismogenic potential, that the presence of potential seismogenic sources in the area should be carefully evaluated.

Offshore CGPS data are crucial to identify, characterize, and quantify the ongoing kinematic processes worldwide, where other measurement methodologies are not applicable, and the only infrastructures are the hydrocarbon platforms. In this work, we show how CGPS data acquired on offshore hydrocarbon platforms can provide useful information on active tectonics even though the geodetic signal could be affected by anthropic activities such as oil/gas exploiting-related deformation.

## Data Availability Statement

All data needed to evaluate the conclusions in the paper are present in the paper itself and/or the associated supporting information. All these data are also freely available in external repositories and previous articles. In particular, the geodetic data are available in Palano et al. (2020) (<https://doi.pangaea.de/10.1594/PANGAEA.914358>). The seismic reflection profiles organized in a 3-D Move<sup>®</sup> file/project are available in Maffucci et al. (2020) (<http://pmd.gfz-potsdam.de/panmetaworks/review/aaf30ce1d97be14e03c64b5a638334ed0c40007bc91f6029b83a149727f47c5f>). Supporting figures (Figures S1 and S2) and tables are available online ([ftp://ftp.ingv.it/pub/giuseppe.pezzo/TECT\\_2020TC006425/](ftp://ftp.ingv.it/pub/giuseppe.pezzo/TECT_2020TC006425/)). In the data repository, we make available the subsurface geophysical data set used to classify the tectonic domains of the studied CGPS stations (i.e., fold-thrust belt, proto-thrust domain, and foreland). The data set is organized into the Move<sup>®</sup> software (Midland Valley) environment, version 2016.2 and includes 60 public 2-D multichannel seismic reflection profiles deriving from the ViDEPI database (<http://www.videpi.com>). The dataset and its full description is available on the following link: <http://doi.org/10.5880/figeo.2020.027> (Maffucci et al., 2020); CGPS data and its full description is available on the following link: <https://doi.org/10.1594/PANGAEA.914358> (Palano et al., 2020).

### Acknowledgments

This research was financed by the Italian Economic Development Ministry in the “CLYPEA-Innovation Network for Future Energy” framework, “subsoil deformations” project, and by Sapienza Università di Roma (Fondi Ateneo 2017 and 2019 to Carminati). We thank Gilberto Dialuce (General Director of DG ISSEG of the Italian Economic Development Ministry) and Franco Terlizze (Director of DGS UNMIG of the Italian Economic Development Ministry) who designed and encouraged the CLYPEA project, creating a successful synergy between Sapienza University, CNR-IGAG, INGV, University of Bologna, RSE, Polytechnic of Turin, CNR-IREA, and Emilia Romagna Region. We thank Eni S.p.A for providing GNSS data. Encouragement and continuous support by Claudio Chiarabba were greatly appreciated. Finally, we thank Prof. M. Barchi and an anonymous reviewer for their constructive comments.

### References

- Amadori, C., Toscani, G., Di Giulio, A., Maesano, F. E., D'Ambrogio, C., Ghielmi, M., & Fantoni, R. (2019). From cylindrical to non-cylindrical foreland basin: Pliocene–Pleistocene evolution of the Po Plain–Northern Adriatic basin (Italy). *Basin Research*, *31*(5), 991–1015. <https://doi.org/10.1111/bre.12369>
- Anderlini, L., Serpelloni, E., Tolomei, C., De Martini, P. M., Pezzo, G., Gualandi, A., & Spada, G. (2020). New insights into active tectonics and seismogenic potential of the Italian Southern Alps from vertical geodetic velocities. *Solid Earth*, *11*, 1681–1698. <https://doi.org/10.5194/se-11-1681-2020>
- Antonucci, I., Rossi, G., Ciccone, F., Carminati, E., Morelli, A., Pezzo, G., et al. (2018). Multidisciplinary study on assessment of subsoil deformations caused by offshore hydrocarbon activity in Emilia Romagna region, aimed to develop a methodological approach for an integrated monitoring. In *Abstract in proceedings of 37<sup>th</sup> GNGTS, session 2.3* (pp. 501–504). Bologna.
- Antonucci, I., Rossi, G., Ciccone, F., Grandi, S., Carminati, E., Morelli, A., et al. (2019). Studio Multidisciplinare delle deformazioni del suolo connesse alle attività di produzione di idrocarburi in aree dell'offshore emiliano romagnolo: avanzamento lavori. In *Abstract in proceedings of 36<sup>th</sup> GNGTS, session 2.3* (pp. 513–517). Trieste.
- Argnani, A. (1998). Structural elements of the Adriatic foreland and their relationships with the front of the Apennine fold-and-thrust belt. *Memorie della Società Geologica Italiana*, *52*, 647–654.
- Bally, A. W. (1986). Balanced sections and seismic reflection profiles across the central Apennines. *Memorie della Società Geologica Italiana*, *35*, 257–310.
- Barchi, M. (1998). The CROP 03 profile: A synthesis of results on deep structures of the Northern Apennines. *Memorie della Società Geologica Italiana*, *52*, 383–400.
- Basili, R., & Barba, S. (2007). Migration and shortening rates in the northern Apennines, Italy: Implications for seismic hazard. *Terra Nova*, *19*(6), 462–468. <https://doi.org/10.1111/j.1365-3121.2007.00772.x>
- Battaglia, M., Murray, M. H., Serpelloni, E., & Bürgmann, R. (2004). The Adriatic region: An independent microplate within the Africa-Eurasia collision zone. *Geophysical Research Letters*, *31*, L09605. <https://doi.org/10.1029/2004GL019723>
- Bennett, R. A., Serpelloni, E., Hreinsdóttir, S., Brandon, M. T., Buble, G., Basic, T., et al. (2012). Syn-convergent extension observed using the RETREAT GPS network, northern Apennines Italy. *Journal of Geophysical Research*, *117*, B04408. <https://doi.org/10.1029/2011JB008744>
- Bigi, G., Bonardi, G., Catalano, R., Cosentino, D., Lentini, F., & Parotto, M. (1992). *Structural Model of Italy: Progetto Finalizzato Geodinamica. CNR-GNDT, Rome, scale, 1*.
- Bird, P., Jackson, D. D., Kagan, Y. Y., Kreemer, C., & Stein, R. S. (2015). GEAR1: A global earthquake activity rate model constructed from geodetic strain rates and smoothed seismicity. *Bulletin of the Seismological Society of America*, *105*(5), 2538–2554. <https://doi.org/10.1785/0120150058>
- Bird, P., Kreemer, C., & Holt, W. E. (2010). A long-term forecast of shallow seismicity based on the global strain rate map. *Seismological Research Letters*, *81*, 184–194. <https://doi.org/10.1785/gssrl.81.2.184>
- Camassi, R., Meloni, F., Postpischl, D., & Sangiorgi, A. (1991). I terremoti riminesi del 1916. In D. Postpischl (Ed.), *San Marino e il terremoto, Bologna* (pp. 167–187).
- Carminati, E., Doglioni, C., & Scrocca, D. (2005). Magnitude and causes of long-term subsidence of the Po plain and Venetian region. In C. A. Fletcher, T. Spencer, J. Da Mosto, & P. Campostrini (Eds.), *Flooding and Environmental Challenges for Venice and its Lagoon: State of Knowledge* (pp. 21–28). Cambridge University Press.
- Carminati, E., Enzi, S., & Camuffo, D. (2007). A study on the effects of seismicity on subsidence in foreland basins: An application to the Venice area. *Global and Planetary Change*, *55*(4), 237–250. <https://doi.org/10.1016/j.gloplacha.2006.03.003>
- Carminati, E., Lustrino, M., Cuffaro, M., & Doglioni, C. (2010). Tectonics, magmatism and geodynamics of Italy: What we know and what we imagine. *Journal of the Virtual Explorer*, *36*, Paper 8, Electronic Edition, ISSN 1441–8142. <https://doi.org/10.3809/jvirtex.2010.00226>
- Carminati, E., Lustrino, M., & Doglioni, C. (2012). Geodynamic evolution of the central and western Mediterranean: Tectonics vs. igneous petrology constraints. *Tectonophysics*, *579*, 173–192. <https://doi.org/10.1016/j.tecto.2012.01.026>
- Carminati, E., Martinelli, G., & Severi, P. (2003). Influence of glacial cycles and tectonics on natural subsidence in the Po plain (northern Italy): Insights from 14C ages. *Geochemistry, Geophysics, Geosystems*, *4*(10), 1082. <https://doi.org/10.1029/2002GC000481>
- Carminati, E., Siletto, G. B., & Battaglia, D. (1997). Thrust kinematics and internal deformation in basement-involved fold and thrust belts: The eastern Orobic Alps case (Central Southern Alps, northern Italy). *Tectonics*, *16*(2), 259–271. <https://doi.org/10.1029/96TC03936>
- Casero, P. (2004). Structural setting of petroleum exploration plays in Italy. In *Special Volume of the Italian Geological Society for the IGC* (Vol. 32, pp. 189–199). Florence.
- Castellarin, A., & Vai, G. B. (1986). Southalpine versus Po plain apenninic arcs. In C. Wezel (Ed.), *The Origin of Arcs. Development in Geotectonics* (Vol. 21, pp. 253–280). Elsevier.
- Channell, J. E. T., d'Argenio, B., & Horvath, F. (1979). Adria, the African promontory, in Mesozoic Mediterranean palaeogeography. *Earth-Science Reviews*, *15*(3), 213–292. [https://doi.org/10.1016/0012-8252\(79\)90083-7](https://doi.org/10.1016/0012-8252(79)90083-7)
- Costa, M. (2003). The buried, Apenninic arcs of the Po Plain and northern Adriatic Sea (Italy): A new model. *Bollettino della Società Geologica Italiana*, *122*, 3–23.
- Coward, M. P., De Donatis, M., Mazzoli, S., Paltrinieri, W., & Wezel, F. C. (1999). Frontal part of the northern Apennines fold and thrust belt in the Romagna-Marche area (Italy): Shallow and deep structural styles. *Tectonics*, *18*(3), 559–574. <https://doi.org/10.1029/1999TC900003>
- Cuffaro, M., Riguzzi, F., Scrocca, D., Antonioli, F., Carminati, E., Livani, M., & Doglioni, C. (2010). On the geodynamics of the northern Adriatic plate. *Rendiconti Lincei*, *21*(S1), 253–279. <https://doi.org/10.1007/s12210-010-0098-9>
- D'Agostino, N. (2014). Complete seismic release of tectonic strain and earthquake recurrence in the Apennines (Italy). *Geophysical Research Letters*, *41*(4), 1155–1162. <https://doi.org/10.1002/2014GL059230>
- Dacome, M. C., Miandro, R., Vettorel, M., & Roncari, G. (2015). Subsidence monitoring network: an Italian example aimed at a sustainable hydrocarbon E&P activity. In *Proceedings of the International Association of Hydrological Sciences* (pp. 372–379).
- D'agostino, N., Avallone, A., Cheloni, D., D'anastasio, E., Mantenuto, S., & Selvaggi, G. (2008). Active tectonics of the Adriatic region from GPS and earthquake slip vectors. *Journal of Geophysical Research*, *113*, B12413. <https://doi.org/10.1029/2008JB005860>
- D'agostino, N., Cheloni, D., Mantenuto, S., Selvaggi, G., Michelini, A., & Zuliani, D. (2005). Strain accumulation in the southern Alps (NE Italy) and deformation at the northeastern boundary of Adria observed by CGPS measurements. *Geophysical Research Letters*, *32*, L19306. <https://doi.org/10.1029/2005GL024266>

- Del Ben, A. (2002). *Interpretation of the CROP M-16 Seismic Section in the Central Adriatic Sea* (Vol. 57, pp. 327–333). Memorie Della Società Geologica Italiana.
- Dercourt, J. E. A., Zonenshain, L. P., Ricou, L. E., Kazmin, V. G., Le Pichon, X., Knipper, A. L., et al. (1986). Geological evolution of the Tethys belt from the Atlantic to the Pamirs since the Lias. *Tectonophysics*, 123(1–4), 241–315. [https://doi.org/10.1016/0040-1951\(86\)90199-X](https://doi.org/10.1016/0040-1951(86)90199-X)
- Devoti, R., D'Agostino, N., Serpelloni, E., Pietrantonio, G., Riguzzi, F., Avallone, A., et al. (2017). The mediterranean crustal motion map compiled at INGV. *Annales de Geophysique*, 60(2), S0215. <https://doi.org/10.4401/ag-7059>
- Devoti, R., Riguzzi, F., Cuffaro, M., & Doglioni, C. (2008). New GPS constraints on the kinematics of the Apennines subduction. *Earth and Planetary Science Letters*, 273(1–2), 163–174. <https://doi.org/10.1016/j.epsl.2008.06.031>
- Dewey, J. F., Helman, M. L., Knott, S. D., Turco, E., & Hutton, D. H. W. (1989). Kinematics of the western Mediterranean. *Geological Society, London, Special Publications*, 45(1), 265–283. <https://doi.org/10.1144/GSL.SP.1989.045.01.15>
- Di Bucci, D., & Mazzoli, S. (2002). Active tectonics of the Northern Apennines and Adria geodynamics: New data and a discussion. *Journal of Geodynamics*, 34(5), 687–707. [https://doi.org/10.1016/S0264-3707\(02\)00107-2](https://doi.org/10.1016/S0264-3707(02)00107-2)
- DISS Working group (2018). *Database of Individual Seismogenic Sources (DISS), Version 3.2.1: A Compilation of Potential Sources for Earthquakes Larger Than M 5.5 in Italy and Surrounding Areas*. Roma: Istituto Nazionale di Geofisica e Vulcanologia. <http://diss.rm.ingv.it/diss/>, <https://doi.org/10.6092/INGV.IT-DISS3.2.1>
- Doglioni, C. (1991). A proposal for the kinematic modelling of W-dipping subductions-possible applications to the Tyrrhenian-Apennines system. *Terra Nova*, 3(4), 423–434. <https://doi.org/10.1111/j.1365-3121.1991.tb00172.x>
- Doglioni, C. (1993). Some remarks on the origin of foredeeps. *Tectonophysics*, 228(1–2), 1–20. [https://doi.org/10.1016/0040-1951\(93\)90211-2](https://doi.org/10.1016/0040-1951(93)90211-2)
- Doglioni, C., Barba, S., Carminati, E., & Riguzzi, F. (2015). Fault on-off versus strain rate and earthquakes energy. *Geoscience Frontiers*, 6(2), 265–276. <https://doi.org/10.1016/j.gsf.2013.12.007>
- Doglioni, C., & Prosser, G. (1997). Fold uplift versus regional subsidence and sedimentation rate. *Marine and Petroleum Geology*, 14(2), 179–190. [https://doi.org/10.1016/S0264-8172\(96\)00065-7](https://doi.org/10.1016/S0264-8172(96)00065-7)
- Fantoni, R., & Franciosi, R. (2009). Mesozoic extension and Cenozoic compression in Po Plain and Adriatic foreland. In *Rendiconti online Società Geologica Italiana* (Vol. 9, pp. 28–31).
- Fantoni, R., & Franciosi, R. (2010). Tectono-sedimentary setting of the Po Plain and Adriatic foreland. *Rendiconti Lincei*, 21(S1), 197–209. <https://doi.org/10.1007/s12210-010-0102-4>
- Fialko, Y. (2006). Interseismic strain accumulation and the earthquake potential on the southern San Andreas fault system. *Nature*, 441(7096), 968–971. <https://doi.org/10.1038/nature04797>
- Finetti, I., & Del Ben, R. (2005). Crustal tectono-stratigraphic setting of the Adriatic Sea from new crop seismic data. In I. Finetti (Ed.), *CROP Project, Deep Seismic Exploration of the Central Mediterranean Region and Italy* (pp. 519–548). Elsevier.
- Franciosi, R., & Vignolo, A. (2002). Northern Adriatic Foreland—a Promising Setting for the Southalpine Midtriassic Petroleum System. In *64th EAGE Conference & Exhibition* (Vol. 5). Florence.
- Frepoli, A., & Amato, A. (2000). Spatial variation in stresses in peninsular Italy and Sicily from background seismicity. *Tectonophysics*, 317, (1–2), 109–124.
- Galluzzo, F., & Santantonio, M. (2002). The Sabina plateau: A new element in the Mesozoic palaeogeography of central Apennines. Tectonic studies group meeting, 1997. *Bollettino della Società Geologica Italiana Special*, 1, 561–588.
- Govoni, A., Marchetti, A., de Gori, P., di Bona, M., Lucente, F. P., Improta, L., et al. (2014). The 2012 Emilia seismic sequence (northern Italy): Imaging the thrust fault system by accurate aftershock location. *Tectonophysics*, 622, 44–55. <https://doi.org/10.1016/j.tecto.2014.02.013>
- Gualandi, A., Nichele, C., Serpelloni, E., Chiaraluze, L., Anderlini, L., Latorre, D., et al. (2017). Aseismic deformation associated with an earthquake swarm in the northern Apennines (Italy). *Geophysical Research Letters*, 44, 7706–7714. <https://doi.org/10.1002/2017GL073687>
- Gulick, S. P. S., Bangs, N. L. B., Shipley, T. H., Nakamura, Y., Moore, G., & Kuramoto, S. (2004). Three-dimensional architecture of the Nankai accretionary prism's imbricate thrust zone off Cape Muroto, Japan: Prism reconstruction via an echelon thrust propagation. *Journal of Geophysical Research*, 109, B02105. <https://doi.org/10.1029/2003JB002654>
- Haines, B. J., Desai, S. D., & Born, G. H. (2013). GPS monitoring of vertical seafloor motion at platform harvest. *Advances in Space Research*, 51(8), 1369–1382. <https://doi.org/10.1016/j.asr.2012.11.008>
- Hammond, W. C., Blewitt, G., & Kreemer, C. (2016). GPS imaging of vertical land motion in California and Nevada: Implications for Sierra Nevada uplift. *Journal of Geophysical Research*, 121, 7681–7703. <https://doi.org/10.1002/2016JB013458>
- Handy, M. R., Schmid, S. M., Bousquet, R., Kissling, E., & Bernoulli, D. (2010). Reconciling plate-tectonic reconstructions of Alpine Tethys with the geological-geophysical record of spreading and subduction in the Alps. *Earth-Science Reviews*, 102(3–4), 121–158. <https://doi.org/10.1016/j.earscirev.2010.06.002>
- Kastelic, V., Vannoli, P., Burrato, P., Fracassi, U., Tiberti, M. M., & Valensise, G. (2013). Seismogenic sources in the Adriatic Domain. *Marine and Petroleum Geology*, 42, 191–213. <https://doi.org/10.1016/j.marpetgeo.2012.08.002>
- Kreemer, C., Blewitt, G., Klein, & E. C. (2014). A geodetic plate motion and global strain rate model, *Geochem. Geochemistry, Geophysics, Geosystems*, 15, 3849–3889. <https://doi.org/10.1002/2014GC005407>
- Laubscher, H. P. (1989). The tectonics of the Southern Alps and the Austro-Alpine nappes: A comparison. *Geological Society of London, Special Publication*, 45(1), 229–241. <https://doi.org/10.1144/GSL.SP.1989.045.01.13>
- Livani, M., Scrocca, D., Arecco, P., & Doglioni, C. (2018). Structural and stratigraphic control on salient and recess development along a thrust belt front: The Northern Apennines (Po Plain, Italy). *Journal of Geophysical Research*, 123, 4360–4387. <https://doi.org/10.1002/2017JB015235>
- Maesano, F. E., D'Ambrogio, C., Burrato, P., & Toscani, G. (2015). Slip-rates of blind thrusts in slow deforming areas: Examples from the Po Plain (Italy). *Tectonophysics*, 643, 8–25. <https://doi.org/10.1016/j.tecto.2014.12.007>
- Maesano, F. E., Toscani, G., Burrato, P., Mirabella, F., D'Ambrogio, C., & Basili, R. (2013). Deriving thrust fault slip rates from geological modeling: Examples from the Marche coastal and offshore contraction belt, Northern Apennines, Italy. *Marine and Petroleum Geology*, 42, 122–134. <https://doi.org/10.1016/j.marpetgeo.2012.10.008>
- Maffucci, R., Petracchini, L., Livani, M., Billi, A., Carminati, E., Cuffaro, M., et al. (2020). *Seismic Reflection Profile Dataset in a 3D Environment of the Northern Adriatic Area (Italy)*. GFZ Data Services. <https://doi.org/10.5880/fgdgeo.2020.027>
- Malinverno, A., & Ryan, W. B. (1986). Extension in the Tyrrhenian Sea and shortening in the Apennines as result of arc migration driven by sinking of the lithosphere. *Tectonics*, 5(2), 227–245. <https://doi.org/10.1029/TC005i002p00227>

- Mariotti, G., & Doglioni, C. (2000). The dip of the foreland monocline in the Alps and Apennines. *Earth and Planetary Science Letters*, 181(1–2), 191–202. [https://doi.org/10.1016/S0012-821X\(00\)00192-8](https://doi.org/10.1016/S0012-821X(00)00192-8)
- Massoli, D., Koyi, H. A., & Barchi, M. R. (2006). Structural evolution of a fold and thrust belt generated by multiple décollements: Analogue models and natural examples from the Northern Apennines (Italy). *Journal of Structural Geology*, 28(2), 185–199. <https://doi.org/10.1016/j.jsg.2005.11.002>
- Molin, D., Bernardini, F., Camassi, R., Caracciolo, C. H., Castelli, V., Ercolani, E., & Postpischl, L. (2008). Materiali per un catalogo dei terremoti italiani: revisione della sismicità minore del territorio nazionale. In *Quaderni di Geofisica* (Vol. 57, pp. 75). Roma: Istituto Nazionale di Geofisica e Vulcanologia (INGV).
- Montone, P., & Mariucci, M. T. (2015). P-wave velocity, density, and vertical stress magnitude along the crustal Po Plain (Northern Italy) from sonic log drilling data. *Pure and Applied Geophysics*, 172(6), 1547–1561. <https://doi.org/10.1007/s00024-014-1022-5>
- Montone, P., & Mariucci, M. T. (2016). The new release of the Italian contemporary stress map. *Geophysical Journal International*, 205(3), 1525–1531. <https://doi.org/10.1093/gji/ggw100>
- Moore, G. F., Mikada, H., Moore, J. C., Becker, K., & Taira, A. (2005). Legs 190 and 196 synthesis: Deformation and fluid flow processes in the Nankai Trough accretionary prism. In *Proceedings of the Ocean Drilling Program: Scientific Results* (Vol. 190, pp. 1–26). Texas A & M University.
- Moore, J. C., Moore, G. F., Cochrane, G. R., & Tobin, H. J. (1995). Negative-polarity seismic reflections along faults of the Oregon accretionary prism: Indicators of overpressuring. *Journal of Geophysical Research*, 100(B7), 12,895–12,906. <https://doi.org/10.1029/94JB02049>
- Muttoni, G., Garzanti, E., Alfonsi, L., Cirilli, S., Germani, D., & Lowrie, W. (2001). Motion of Africa and Adria since the Permian: Paleomagnetic and paleoclimatic constraints from northern Libya. *Earth and Planetary Science Letters*, 192(2), 159–174. [https://doi.org/10.1016/S0012-821X\(01\)00439-3](https://doi.org/10.1016/S0012-821X(01)00439-3)
- Okada, Y. (1985). Surface deformation due to shear and tensile faults in a half-space. *Bulletin of the Seismological Society of America*, 75(4), 1135–1154.
- Palano, M., Pezzo, G., Serpelloni, E., Devoti, R., D'Agostino, N., Gandolfi, S., et al. (2020). Geopositioning Time Series from Offshore Platforms in the Adriatic Sea. *Scientific Data*. <https://doi.org/10.1038/s41597-020-00705-w>
- Patacca, E., Sartori, R., & Scandone, P. (1990). Tyrrhenian basin and Apenninic arcs: Kinematic relations since Late Tortonian times. *Memorie della Società Geologica Italiana*, 45, 425–451.
- Perotti, C. R. (1991). Osservazioni sull'assetto strutturale del versante padano dell'Appennino nordoccidentale. *Atti Ticinesi Scienze della Terra*, 34, 11–22. *Rendiconti Lincei*, 21(1), 253–279.
- Petricca, P., Carminati, E., & Doglioni, C. (2019). The decollement depth of active thrust faults in Italy: Implications on potential earthquake magnitude. *Tectonics*, 38(11), 3990–4009. <https://doi.org/10.1029/2019TC005641>
- Petricca, P., Carminati, E., Doglioni, C., & Riguzzi, F. (2018). Brittle-ductile transition depth versus convergence rate: Impact on seismicity. *Physics of the Earth and Planetary Interiors*, 284. <https://doi.org/10.1016/j.pepi.2018.09.002>
- Pezzo, G., De Gori, P., Lucente, F. P., & Chiarabba, C. (2018). Pore pressure pulse drove the 2012 Emilia (Italy) series of earthquakes. *Geophysical Research Letters*, 45, 682–690. <https://doi.org/10.1002/2017GL076110>
- Pezzo, G., Merryman Boncori, J. P., Tolomei, C., Salvi, S., Atzori, S., Antonioli, A., et al. (2013). Coseismic deformation and source modeling of the May 2012 Emilia (Northern Italy) earthquakes. *Seismological Research Letters*, 84(4), 645–655. <https://doi.org/10.1785/0220120171>
- Pezzo, G., Tolomei, C., Atzori, S., Salvi, S., Shabanian, E., Bellier, O., & Farbod, Y. (2012). New kinematic constraints of the western Doruneh fault, northeastern Iran, from interseismic deformation analysis. *Geophysical Journal International*, 190(1), 622–628. <https://doi.org/10.1111/j.1365-246X.2012.05509.x>
- Pieri, M., & Groppi, G. (1981). *Subsurface geological structure of the Po Plain: CNR* (Vol. 414, p. 23). Pubblicazione del Progetto Finalizzato Geodinamica.
- Ponraj, M., Amirtharaj, S., Sunil, P. S., Saji, A. P., Kumar, K. V., Arora, S. K., et al. (2019). An assessment of present-day crustal deformation in the Kumaun Himalaya from GPS observations. *Journal of Asian Earth Sciences*, 176, 274–280. <https://doi.org/10.1016/j.jseas.2019.02.019>
- Ricci Lucchi, F. (1986). The foreland basin system of the Northern Apennines and related clastic wedges: A preliminary outline. *Giornale di Geologia*, 48(3), 165–185.
- Riguzzi, F., Crespi, M., Devoti, R., Doglioni, C., Pietrantonio, G., & Pisani, A. R. (2012). Geodetic strain rate and earthquake size: New clues for seismic hazard studies. *Physics of the Earth and Planetary Interiors*, 206, 67–75. <https://doi.org/10.1016/j.pepi.2012.07.005>
- Roeder, D. (1989). South-Alpine thrusting and trans-Alpine convergence. In M. P. Coward (Ed.), *Alpine tectonics* (Vol. 45, pp. 211–227). Geological Society of London Special Publication. <https://doi.org/10.1144/GSL.SP.1989.045.01.12>
- Roveri, M., Bassetti, M. A., & Ricci Lucchi, F. (2001). The Mediterranean Messinian salinity crisis: An Apennine foredeep perspective. *Sedimentary Geology*, 140(3–4), 201–214. [https://doi.org/10.1016/S0037-0738\(00\)00183-4](https://doi.org/10.1016/S0037-0738(00)00183-4)
- Rovida, A., Locati, M., Camassi, R., Lolli, B., & Gasperini, P. (2020). The Italian earthquake catalogue CPTI15. *Bulletin of Earthquake Engineering*, 18(7), 2953–2984. <https://doi.org/10.1007/s10518-020-00818-y>
- Schmid, S. M., Bernoulli, D., Fügenschuh, B., Matenco, L., Schefer, S., Schuster, R., et al. (2008). The Alpine-Carpathian-Dinaridic orogenic system: Correlation and evolution of tectonic units. *Swiss Journal of Geosciences*, 101(1), 139–183. <https://doi.org/10.1007/s00015-008-1247-3>
- Scisciani, V. (2009). Styles of positive inversion tectonics in the Central Apennines and in the Adriatic foreland: Implications for the evolution of the Apennine chain (Italy). *Journal of Structural Geology*, 31(11), 1276–1294. <https://doi.org/10.1016/j.jsg.2009.02.004>
- Scrocca, D. (2006). Thrust front segmentation induced by differential slab retreat in the Apennines (Italy). *Terra Nova*, 18(2), 154–161. <https://doi.org/10.1111/j.1365-3121.2006.00675.x>
- Scrocca, D., Carminati, E., Doglioni, C., & Marcantoni, D. (2007). Slab retreat and active shortening along the central-northern Apennines. In *Thrust belts and foreland basins* (pp. 471–487). Berlin, Heidelberg: Springer. [https://doi.org/10.1007/978-3-540-69426-7\\_25](https://doi.org/10.1007/978-3-540-69426-7_25)
- Selli, R. (1973). *An outline of the Italian Messinian. Koninklijke Nederlandse Akademie Van Wetenschappen: Messinian Events in the Mediterranean Geodynamics*, Scientific Report no. 7 of the Colloquium held in Utrecht, 2–4 March (pp. 150–171).
- Suppe, J., & Medwedeff, D. A. (1990). Geometry and kinematics of fault-propagation folding. *Eclogae Geologicae Helveticae*, 83(3), 409–454.
- Toda, S., Stein, R. S., Sevilgen, V., & Lin, J. (2011). *Coulomb 3.3 Graphic-Rich Deformation and Stress-Change Software for Earthquake, Tectonic, and Volcano Research and Teaching—User Guide*. U.S. Geological Survey, Open-File Report 2011–1060 (p. 63). Available at <http://pubs.usgs.gov/of/2011/1060/>

- Toscani, G., Marchesini, A., Barbieri, C., Di Giulio, A., Fantoni, R., Mancin, N., & Zanferrari, A. (2016). The Friulian-Venetian Basin I: Architecture and sediment flux into a shared foreland basin. *Italian Journal of Geosciences*, *135*(3), 444–459. <https://doi.org/10.3301/IJG.2015.35>
- Turrini, C., Angeloni, P., Lacombe, O., Ponton, M., & Roure, F. (2015). Three-dimensional seismo-tectonics in the Po Valley basin, Northern Italy. *Tectonophysics*, *661*, 156–179. <https://doi.org/10.1016/j.tecto.2015.08.033>
- Turrini, C., Toscani, G., Lacombe, O., & Roure, F. (2016). Influence of structural inheritance on foreland-foredeep system evolution: An example from the Po Valley region (northern Italy). *Marine and Petroleum Geology*, *77*, 376–398. <https://doi.org/10.1016/j.marpetgeo.2016.06.022>
- Vannoli, P., Basili, R., & Valensise, G. (2004). New geomorphic evidence for anticlinal growth driven by blind-thrust faulting along the northern Marche coastal belt (central Italy). *Journal of Seismology*, *8*(3), 297–312. <https://doi.org/10.1023/B:JOSE.0000038456.00574.e3>
- Vergne, J., Cattin, R., & Avouac, J. P. (2001). On the use of dislocations to model interseismic strain and stress build-up at intracontinental thrust faults. *Geophysical Journal International*, *147*(1), 155–162. <https://doi.org/10.1046/j.1365-246X.2001.00524.x>
- Wrigley, R., Hodgson, N., & Eestime, P. (2015). Petroleum geology and hydrocarbon potential of the Adriatic basin, offshore Croatia. *Journal of Petroleum Geology*, *38*, 301–316. <https://doi.org/10.1111/jpg.12612>